Sensitivity of the transverse flow to the symmetry energy

Sakshi Gautam,[1] Aman D. Sood,[2] Rajeev K. Puri,[1,*] and J. Aichelin[2]

[1]*Department of Physics, Panjab University, Chandigarh 160 014, India*

[2]*SUBATECH, Laboratoire de Physique Subatomique et des Technologies Associées, Université de Nantes, IN2P3/CNRS,*
École des Mines de Nantes, 4 rue Alfred Kastler, F-44072 Nantes, France

We study the sensitivity of transverse flow to symmetry energy in the Fermi energy region as well as at high energies. We find that transverse flow is sensitive to symmetry energy and its density dependence in the Fermi energy region. We also show that the transverse flow can address the symmetry energy at densities about twice the saturation density; however, it shows insensitivity to the symmetry energy at densities $\rho/\rho_0 > 2$. The mechanism for the sensitivity of transverse flow to symmetry energy and its density dependence is also discussed.

PACS number(s): 21.65.Ef, 24.10.Lx, 25.70.−z, 25.75.Ld

I. INTRODUCTION

Heavy-ion collisions (HIC) are the only method presently available in the laboratory to produce large volume of excited nuclear matter. The production of such state is essential not only to investigate the gross characteristics of nuclear matter but also to explore the explosion mechanism of supernovas and the cooling rate of neutron stars. After about three decades of extensive efforts in both nuclear experiments and theoretical calculations, the equation of state (EOS) of isospin symmetric matter is well understood through experiments of collective flow [1] and subthreshold kaon production [2,3]. Nowadays, the nuclear EOS of asymmetric nuclear matter has attracted a lot of attention. The EOS of asymmetric nuclear matter can be described approximately by

$$E(\rho, \delta) = E_0(\rho, \delta = 0) + E_{\text{sym}}(\rho)\delta^2, \tag{1}$$

where $\delta = \frac{\rho_n - \rho_p}{\rho_n + \rho_p}$ is isospin asymmetry, $E_0(\rho, \delta)$ is the energy of pure symmetric nuclear matter, and $E_{\text{sym}}(\rho)$ is the symmetry energy, where $E_{\text{sym}}(\rho_0) = 32$ MeV is the symmetry energy at normal nuclear matter density. The symmetry energy is $E(\rho, 1) - E_0(\rho, 0)$, i.e., the difference of the energy per nucleon between pure neutron matter and symmetric nuclear matter. The symmetry energy is important not only to the nuclear physics community as it sheds light on the structure of radioactive nuclei and reaction dynamics induced by rare isotopes, but also to astrophysicists since it acts as a probe for understanding the evolution of massive stars and supernova explosions [4]. The existing and upcoming radioactive ion beam (RIB) facilities lead a way in understanding nuclear symmetry energy. Experimentally, symmetry energy is not a directly measurable quantity and has to be extracted from observables which are related to symmetry energy. Therefore, a crucial task is to find such observables which can shed light on symmetry energy. A large number of studies on the symmetry energy of nuclear matter have been done during the past decade [5–11]. These studies reveal that in heavy-ion collisions induced by neutron-rich nuclei, the effect of nuclear symmetry energy can be studied via the

preequilibrium n/p ratio [5–7], isospin fractionation [8,9], n-p differential transverse flow [10,11], and so on. These observables have their relative importance depending on the region of density one wants to explore. For example, below saturation density ($0.3\rho_0 \leqslant \rho \leqslant \rho_0$), observables such as fragment yield, the isoscaling parameter, isospin diffusion, and the double n-p ratio have been used to extract symmetry energy. On the other extreme, the π^+/π^- ratio, the relative and differential collective flow between triton/He^3, and the n-p differential collective flow act as probes of symmetry energy at high densities. In the low density region, Shetty *et al.* [12] extracted the symmetry energy by comparing the isoscaling parameters from ^{40}Ar, ^{40}Ca+^{58}Fe, ^{58}Ni and ^{58}Fe, ^{58}Ni+^{58}Fe, ^{58}Ni reactions with dynamical antisymmetrized molecular dynamics (AMD) calculations [13] and found it to be of the form $E_{\text{sym}} = 31.6(\frac{\rho}{\rho_0})^\gamma$, with $\gamma = 0.69$. Famiano *et al.* [14] studied the symmetry energy by comparing the experimental double neutron to proton ratio in ^{112}Sn+^{112}Sn and ^{124}Sn+^{124}Sn reactions with isospin-dependent Boltzmann-Uehling-Uhlenbeck (IBUU) calculations [15] and obtained the form $E_{\text{sym}} = 32(\frac{\rho}{\rho_0})^\gamma$, $\gamma = 0.5$. Recently Tsang *et al.* [7] compared the isospin diffusion and n-p double ratio for ^{124}Sn+^{112}Sn reaction with isospin-dependent quantum molecular dynamics (IQMD) calculations [16] and obtained a similar form of symmetry energy with $\gamma = 0.4$–1.05. The situation is worse at higher densities. The results are model dependent and also contradictory. The FOPI collaboration at GSI studied the π^+/π^- ratio in ^{40}Ca+^{40}Ca, ^{96}Ru+^{96}Ru, ^{96}Zr+^{96}Zr, and ^{197}Au+^{197}Au reactions [17]. A comparison of this data [18] with IBUU calculations showed a softer form of the density dependence of symmetry energy, which is in contrast to those obtained from the low density studies where stiffer form of symmetry energy reproduced the data well. The π^+/π^- ratio was also compared with improved quantum molecular dynamics (ImQMD) calculations by Feng *et al.* [19] and favored a stiffer form of symmetry energy and was in contradiction with IBUU calculations. At densities higher than saturation density, collective flow has also been proposed as a novel means to probe the high density behavior of symmetry energy [10]. In this paper, we aim to see the sensitivity of collective transverse in-plane flow to symmetry energy and also to see the effect of different density dependencies of
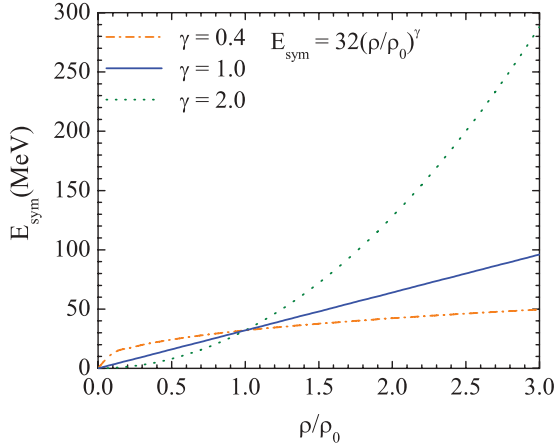
---

*rkpuri@pu.ac.in

FIG. 1. (Color online) The density dependence of symmetry energy for various forms of symmetry energy: F_1 ($\gamma = 1.0$) (solid), F_2 ($\gamma = 0.4$) (dashed), and F_3 ($\gamma = 2.0$) (dotted).

symmetry energy on the same. The various forms of symmetry energy used in present study are $E_{\text{sym}} \propto F_1(u)$, $E_{\text{sym}} \propto F_2(u)$, and $E_{\text{sym}} \propto F_3(u)$, where $u = \frac{\rho}{\rho_0}$, $F_1(u) \propto u$, $F_2(u) \propto u^{0.4}$, $F_3(u) \propto u^2$, and F_4 represents calculations without symmetry energy. The different density dependencies of symmetry energy are shown in Fig. 1. The various lines are explained in the caption of the figure. Section II describes the model in brief. Section III explains the results and gives our discussion, and Sec. IV summarizes the results.

II. THE MODEL

The present study is carried out within the framework of the isospin-dependent quantum molecular dynamics (IQMD) model [20]. The IQMD model treats different charge states of nucleons, deltas, and pions explicitly, as inherited from the Vlasov-Uehling-Uhlenbeck (VUU) model. The IQMD model has been used successfully for the analysis of a large number of observables from low to relativistic energies. The isospin degree of freedom enters into the calculations via symmetry potential, cross sections, and Coulomb interaction.

In this model, baryons are represented by Gaussian-shaped density distributions:

$$f_i(\vec{r}, \vec{p}, t) = \frac{1}{\pi^2 \hbar^2} \exp\left(-[\vec{r} - \vec{r}_i(t)]^2 \frac{1}{2L}\right)$$
$$\times \exp\left(-[\vec{p} - \vec{p}_i(t)]^2 \frac{2L}{\hbar^2}\right). \quad (2)$$

Nucleons are initialized in a sphere with radius $R = 1.12 A^{1/3}$ fm, in accordance with liquid-drop model. Each nucleon occupies a volume of h^3, so that phase space is uniformly filled. The initial momenta are randomly chosen between 0 and Fermi momentum ($\vec{p}_F$). The nucleons of the target and projectile interact by two- and three-body Skyrme forces, the Yukawa potential, and Coulomb interactions. In addition to the use of explicit charge states of all baryons and mesons, a symmetry potential between protons and neutrons corresponding to the Bethe-Weizsäcker mass formula has been included. The

hadrons propagate using Hamilton equations of motion:

$$\frac{d\vec{r}_i}{dt} = \frac{d\langle H \rangle}{d\vec{p}_i}, \quad \frac{d\vec{p}_i}{dt} = -\frac{d\langle H \rangle}{d\vec{r}_i} \quad (3)$$

with

$$\langle H \rangle = \langle T \rangle + \langle V \rangle$$
$$= \sum_i \frac{p_i^2}{2m_i} + \sum_i \sum_{j>i} \int f_i(\vec{r}, \vec{p}, t) V^{ij}(\vec{r}', \vec{r})$$
$$\times f_j(\vec{r}', \vec{p}', t) \, d\vec{r} \, d\vec{r}' \, d\vec{p} \, d\vec{p}'. \quad (4)$$

The baryon potential V^{ij} in the above relation reads as

$$V^{ij}(\vec{r}' - \vec{r}) = V^{ij}_{\text{Skyrme}} + V^{ij}_{\text{Yukawa}} + V^{ij}_{\text{Coul}} + V^{ij}_{\text{sym}}$$
$$= \left[t_1 \delta(\vec{r}' - \vec{r}) + t_2 \delta(\vec{r}' - \vec{r}) \rho^{\gamma-1} \left(\frac{\vec{r}' + \vec{r}}{2} \right) \right]$$
$$+ t_3 \frac{\exp(|(\vec{r}' - \vec{r})|/\mu)}{(|(\vec{r}' - \vec{r})|/\mu)} + \frac{Z_i Z_j e^2}{|(\vec{r}' - \vec{r})|}$$
$$+ t_4 \frac{1}{\varrho_0} T_{3i} T_{3j} \delta(\vec{r}_i' - \vec{r}_j). \quad (5)$$

Here Z_i and Z_j denote the charges of ith and jth baryon, and T_{3i} and T_{3j} are their respective T_3 components (i.e., $1/2$ for protons and $-1/2$ for neutrons). The parameters μ and $t_1, \ldots, t_4$ are adjusted to the real part of the nucleonic optical potential. For the density dependence of the nucleon optical potential, standard Skyrme type parametrization is employed.

III. RESULTS AND DISCUSSION

We simulate several thousands events for the neutron-rich system of ^{48}Ca+^{48}Ca and ^{60}Ca+^{60}Ca at energies of 100, 400, and 800 MeV/nucleon at an impact parameter of $b/b_{\text{max}} = 0.2$–0.4. We use a soft equation of state and an isospin- and energy-dependent cross section reduced by 20%; i.e., $\sigma = 0.8\sigma_{nn}^{\text{free}}$. The details about the elastic and inelastic cross sections for proton-proton and proton-neutron collisions can be found in [20,21]. The cross section for neutron-neutron collisions is assumed to be equal to the proton-proton cross section.

Since ^{60}Ca has a very high asymmetry, to ensure the stability of the nuclei in the present study, we display in Fig. 2 the time evolution of the root mean square radius of a single nucleus of ^{40}Ca (solid line), ^{48}Ca (dashed), and ^{60}Ca (dotted) in the coordinate [Fig. 2(a)] and momentum space [Fig. 2(b)]. The results are displayed for nuclei intialized with symmetry energy $F_1(u)$. We find that the stability is of the same order for all three nuclei.

There are several methods used in the literature to define the nuclear transverse in-plane flow. In most of the studies, one uses (p_x/A) plots where one plots (p_x/A) as a function of $Y_{\text{cm}}/Y_{\text{beam}}$. Using a linear fit to the slope, one can define the so-called reduced flow (F). Alternatively, one can also use a more integrated quantity "directed transverse in-plane flow" $\langle p_x^{\text{dir}} \rangle$ which is defined as [20]

$$\langle p_x^{\text{dir}} \rangle = \frac{1}{A} \sum_i \text{sign}\{Y(i)\} p_x(i), \quad (6)$$
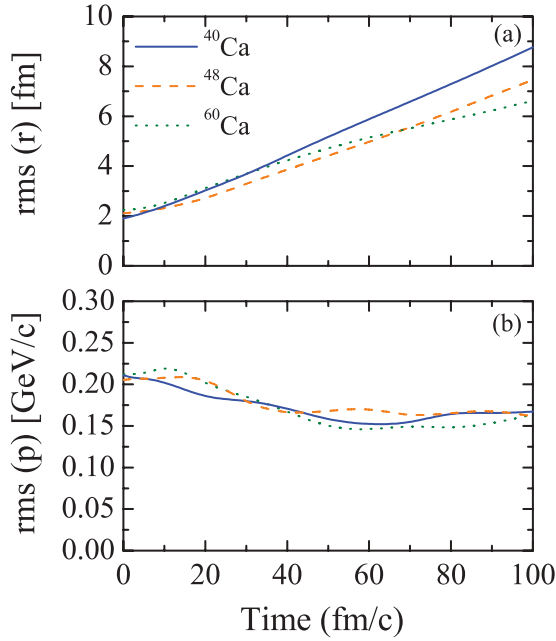
FIG. 2. (Color online) Time evolution of root mean square radius of single ^{40}Ca, ^{48}Ca, and ^{60}Ca nuclei in coordinate (top panel) and momentum space (bottom panel) obtained with IQMD for EOS used in the present study for symmetry energy $F_1(u)$.

FIG. 3. (Color online) Left panels: $\langle \frac{p_x}{A} \rangle$ as a function of Y_{cm}/Y_{beam} for different energies of 100, 400, and 800 MeV/nucleon for different forms of symmetry energy. Right panels: The time evolution of $\langle p_x^{dir} \rangle$ at 100, 400, and 800 MeV/nucleon for different forms of symmetry energy at $b/b_{max} = 0.2$–0.4. Lines are explained in the text.

where $Y(i)$ and $p_x(i)$ are the rapidity distribution and transverse momentum of the ith particle. In this definition, all rapidity bins are taken into account. It therefore presents an easier way of measuring the in-plane flow than complicated functions such as (p_x/A) plots.

In Fig. 3 we display $\langle \frac{p_x}{A} \rangle$ as a function of Y_{cm}/Y_{beam} at final time (left panels) and the time evolution of $\langle p_x^{dir} \rangle$ (right panels) calculated at 100 (top panel), 400 (middle), and 800 MeV/nucleon (bottom) for different density dependencies of symmetry energy. Solid, dash dotted, and dotted lines represent the symmetry energy proportional to ρ, $\rho^{0.4}$, and ρ^2, whereas the dashed line represents calculations without symmetry energy. Comparing the left and right panels in Fig. 3, we find that both the methods show similar behavior to symmetry energy. For example, at incident energy of 100 MeV/nucleon for $E_{sym} \propto \rho^{0.4}$, $\langle p_x^{dir} \rangle = 0$. Similarly, the slope of $\langle \frac{p_x}{A} \rangle$ at midrapidity is zero. We also find that the transverse momentum is sensitive to symmetry energy and to its density dependencies $F_1(u)$, $F_2(u)$, and $F_3(u)$ in the low energy region (100 MeV/nucleon). At energies above Fermi energy, both the methods show insensitivity to the different symmetry energies. This is because the repulsive n-n scattering dominates the mean field at high energies.

To understand the sensitivity of transverse momentum to the symmetry energy as well as its density dependence in the Fermi energy region, we calculate the transverse flow as well as rapidity distribution of particles having $\frac{\rho}{\rho_0} < 1$ (denoted as bin 1) and particles having $\frac{\rho}{\rho_0} \geqslant 1$ (bin 2) separately at all the time steps. Since both the methods show similar behavior to symmetry energy, for simplicity the following discussion will be in terms of $\langle p_x^{dir} \rangle$.
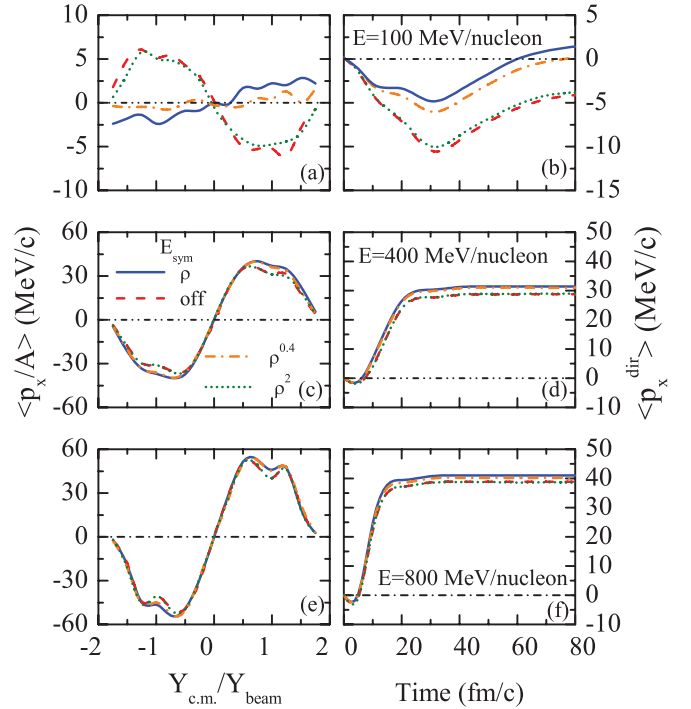
In Fig. 4 we display the rapidity distributions at 100 MeV/nucleon of all the particles (dotted line), particles corresponding to bin 1 (solid), and to bin 2 (dashed) at 0, 10, 20, 30, 40, and 60 fm/c. We have calculated rapidity distributions for different forms of symmetry energy used in this paper. We find that they are insensitive to the symmetry energy [22,23]. In Fig. 4, we display the rapidity distribution calculated without symmetry energy. During the initial stages we see the two Gaussians at projectile and target rapidities for all three bins. The peaks of the Gaussians will be more prominent at higher energies. The interest for our discussion is in bin 1 and bin 2. During the start of the reaction (0 fm/c) a higher number of particles lie in bin 1; i.e., a higher number of particles have $\frac{\rho}{\rho_0} < 1$. As the nuclei begin to overlap, the density increases in the overlap zone. Now, the number of particles increases in bin 2 (at 10 fm/c). From 10 to 20 fm/c, the number of particles continue increasing in bin 2 at midrapidity; i.e., particles from large rapidity continue shifting to bin 2 in the midrapidity region. This is expected since at incident energies in the Fermi energy region dynamics is governed by the attractive mean field. The dominance of the attractive mean field will prompt the deflection of particles into negative angles, i.e., toward the participant zone. After 20–30 fm/c, the expansion phase of the reaction begins and the number of particles continues increasing in bin 1, and by 60 fm/c most of the particles lie in bin 1.

In Fig. 5 we display the time evolution of $\langle p_x^{dir} \rangle$ for different symmetry energies used in this paper at 100 MeV/nucleon
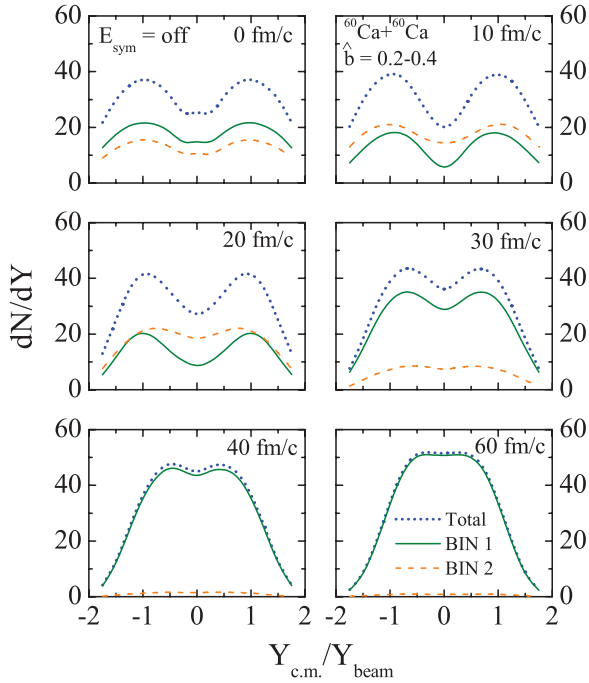
FIG. 4. (Color online) The time evolution of rapidity distribution for the calculations with no symmetry energy for various bins at $b/b_{max} = 0.2$–0.4. Lines are explained in the text.

for particles lying in the different bins. Lines have the same meaning as in Fig. 4. Panels (a), (b), and (c) are for $E_{sym} \propto \rho$, $\rho^{0.4}$, and ρ^2, respectively. Panel (d) is for calculations without symmetry energy. The total $\langle p_x^{dir} \rangle$ is negative during the initial stages and continues decreasing till 30 fm/c which indicates dominance of attractive interaction. In panels (a) and (b), it becomes positive whereas in panels (c) and (d) it remains negative during the course of the reaction. If we look at $\langle p_x^{dir} \rangle$ of particles lying in bin 1 for $F_1(u)$ [Fig. 5(a)] and $F_2(u)$ [Fig. 5(b)] in the time interval 0 to about

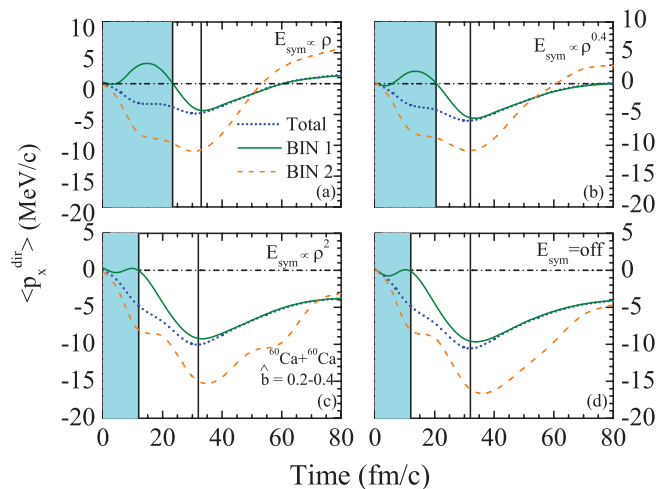20–25 fm/c, we see that it remains positive. It increases with time up to 15 fm/c and reaches a peak value. This is because in the spectator region (where high rapidity particles lie) the repulsive symmetry energy will accelerate the particles away from the overlap zone in the transverse direction. After 15 fm/c, $\langle p_x^{dir} \rangle$ (of particles in bin 1) begins to decrease. This is because these particles will now be attracted toward the central dense zone. As shown in Fig. 4, from 10 to 20 fm/c particles in bin 2 continue increasing in the midrapidity region. In the case of $F_1(u)$ and $F_2(u)$, particles which enter the central dense zone (bin 2) already have a high positive value of $\langle p_x^{dir} \rangle$ (i.e., going away from the dense zone). So, the attractive mean field has to decelerate the particles first, make them stop, and then accelerate the particles back toward the overlap zone. At about 20–25 fm/c particles from bin 1 have zero $\langle p_x^{dir} \rangle$ [see shaded area in Figs. 5(a) and 5(b)]. Up to 30 fm/c, particles feel the attractive mean field potential after which the high density phase is over; i.e., in the case of $F_1(u)$ and $F_2(u)$ between 0 and 30 fm/c particles from bin 1 are accelerated toward the overlap zone only for a short time interval of about 5 fm/c, whereas for the case of $F_3(u)$ [Fig. 5(c)] and F_4 [Fig. 5(d)] between 0 and 30 fm/c, particles from bin 1 are accelerated toward the overlap zone for a longer time interval of about 20 fm/c between 10–30 fm/c. Moreover, the $\langle p_x^{dir} \rangle$ of particles lying in bin 1 [for $F_3(u)$ and F_4] follows a similar trend. This is because for $\rho/\rho_0 < 1$ the strength of symmetry energy $F_3(u)$ will be small and so there will be less effect of symmetry energy on the particles, which is evident from Fig. 5(c), where one sees that the $\langle p_x^{dir} \rangle$ remains about zero during the initial stages between zero to about 10 fm/c.

FIG. 5. (Color online) The time evolution of $\langle p_x^{dir} \rangle$ for different forms of symmetry energy for different bins at $b/b_{max} = 0.2$–0.4. Lines have the same meaning as in Fig. 4.
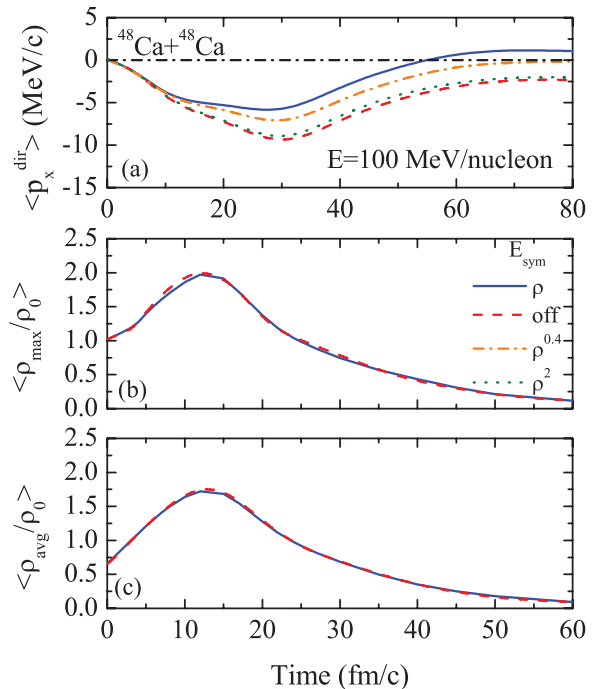

FIG. 6. (Color online) (a) The time evolution of $\langle p_x^{dir} \rangle$ at 100 MeV/nucleon for different forms of symmetry energy for ^{48}Ca+^{48}Ca. (b) The time evolution of $\langle \rho_{max}/\rho_0 \rangle$ and (c) $\langle \rho_{avg}/\rho_0 \rangle$ for $F_1(u)$ and F_4. Lines have same meaning as in Fig. 3.

The $\langle p_x^{\mathrm{dir}} \rangle$ due to particles in bin 2 (dashed line) decreases in a very similar manner for all four different symmetry energies between 0 and 10 fm/c. Between 10 and 25 fm/c, $\langle p_x^{\mathrm{dir}} \rangle$ for $F_3(u)$ and F_4 decreases more sharply as compared to the case of $F_1(u)$ and $F_2(u)$. This is because in this time interval particles from bin 1 enter into bin 2. As discussed earlier, $\langle p_x^{\mathrm{dir}} \rangle$ of particles entering bin 2 from bin 1 in the case of $F_1(u)$ and $F_2(u)$ will be less negative due to the stronger effect of symmetry energy as compared to the case of $F_3(u)$ and F_4.

Since the reaction ^{60}Ca+^{60}Ca is an extreme case with large isospin asymmetry, to check whether the above predicted effects survive in reactions which are experimentally accessible, we simulate the reaction of ^{48}Ca+^{48}Ca for all the different forms of symmetry energy used in the present study. The reaction ^{48}Ca+^{48}Ca has been used in many previous studies [24]. The results are shown in Fig. 6(a). We find that even for this reaction the transverse flow shows sensitivity to symmetry energy and its density dependence. In Figs. 6(b) and 6(c), we display the time evolution of maximum density $\langle \rho_{\mathrm{max}}/\rho_0 \rangle$ and average density $\langle \rho_{\mathrm{avg}}/\rho_0 \rangle$, respectively, at 100 MeV/nucleon. We find that the density reached is about 2.0 times the saturation density. Moreover, the maximal density is reached in the time interval 0–30 fm/c, and the effect of symmetry energy on $\langle p_x^{\mathrm{dir}} \rangle$ of particles during this interval

decides the fate of the final value of $\langle p_x^{\mathrm{dir}} \rangle$. Thus transverse flow can address the symmetry energy at densities about 2.0 times the saturation density.

IV. SUMMARY

We have checked the sensitivity of transverse flow to symmetry energy in the Fermi energy region as well as at high energies. We have found that transverse flow is sensitive to symmetry energy as well as to its density dependence in the Fermi energy region. We have also shown that the transverse flow can address the symmetry energy at densities about twice the saturation density; however, it shows insensitivity to symmetry energy at densities $\rho/\rho_0 > 2$. We have also discussed the mechanism for the sensitivity of transverse flow to symmetry energy and to its density dependence.

ACKNOWLEDGMENTS

[1] W. Scheid, H. Müller, and W. Greiner, Phys. Rev. Lett. **32**, 741 (1974); H. A. Gustafsson et al., *ibid.* **52**, 1590 (1984); K. G. R. Doss *et al.*, *ibid.* **57**, 302 (1986).

[2] D. Klakow, G. Welke, and W. Bauer, Phys. Rev. C **48**, 1982 (1993).

[3] C. Hartnack, J. Jaenicke, L. Sehn, H. Stöcker, and J. Aichelin, Nucl. Phys. A **580**, 643 (1994).

[4] S. Kubis, Phys. Rev. C **76**, 025801 (2007); G. F. Marranghello, C. Providência, and A. M. S. Santos, *ibid.* **81**, 024307 (2010).

[5] Y. Zhang and Z. Li, Phys. Rev. C **71**, 024604 (2005).

[6] Q. Li, Z. Li, and H. Stöcker, Phys. Rev. C **73**, 051601(R) (2006).

[7] M. B. Tsang, Y. Zhang, P. Danielewicz, M. Famiano, Z. Li, W. G. Lynch, and A. W. Steiner, Phys. Rev. Lett. **102**, 122701 (2009).

[8] B. A. Li and C. M. Ko, Nucl. Phys. A **618**, 498 (1997).

[9] V. Baran, M. Colonna, M. Di Toro, and A. B. Laroinov, Nucl. Phys. A **632**, 287 (1999).

[10] B. A. Li, Phys. Rev. Lett. **88**, 192701 (2002).

[11] B. A. Li, Phys. Rev. C **69**, 034614 (2004).

[12] D. V. Shetty, S. J. Yennello, A. S. Botvina, G. A. Souliotis, M. Jandel, E. Bell, A. Keksis, S. Soisson, B. Stein, and J. Iglio, Phys. Rev. C **70**, 011601 (2004).

[13] A. Ono, P. Danielewicz, W. A. Friedman, W. G. Lynch, and M. B. Tsang, Phys. Rev. C **68**, 051601 (2003).

[14] M. A. Famiano *et al.*, Phys. Rev. Lett. **97**, 052701 (2006).

[15] B. A. Li, C. M. Ko, and Z. Ren, Phys. Rev. Lett. **78**, 1644 (1997).

[16] Y. Zhang, P. Danielewicz, M. Famiano, Z. Li, W. G. Lynch, and M. B. Tsang, Phys. Lett. B **664**, 145 (2008).

[17] W. Reisdorf *et al.*, Nucl. Phys. A **781**, 459 (2007).

[18] Z. Xiao, B. A. Li, L. W. Chen, G. C. Yong, and M. Zhang, Phys. Rev. Lett. **102**, 062502 (2009).

[19] Z. Feng and G. M. Jin, Phys. Lett. B **683**, 140 (2010).

[20] C. Hartnack, R. K. Puri, J. Aichelin, J. Konopka, S. A. Bass, H. Stöcker, and W. Greiner, Eur. Phys. J. A **1**, 151 (1998).

[21] J. Cugnon, T. Mizutani, and J. Vandermeulen, Nucl. Phys. A **352**, 505 (1981).

[22] G. Lehaut *et al.*, Phys. Rev. Lett **104**, 232701 (2010).

[23] S. Kumar, S. Kumar, and R. K. Puri, Phys. Rev. C **81**, 014601 (2010).

[24] M. C. Wang, W. H. Ling, W. J. Yang, and L. G. Jie, Chin. Phys. B **18**, 4781 (2009); L. W. Chen, C. M. Ko, and B. A. Li, Phys. Rev. C **68**, 017601 (2003).